Quantum inelastic electron–vibration scattering in molecular wires: Landauer-like versus Green's function approaches and temperature effects

2006 J. Phys.: Condens. Matter 18 6307

(http://iopscience.iop.org/0953-8984/18/27/014)

INSTITUTE OF PHYSICS PUBLISHING JOURNAL OF PHYSICS: CONDENSED MATTER

J. Phys.: Condens. Matter **18** (2006) 6307–6328 doi:10.1088/0953-8984/18/27/014

Quantum inelastic electron–vibration scattering in molecular wires: Landauer-like versus Green's function approaches and temperature effects

H Ness

CEA-Saclay, Service de Physique et Chimie des Surfaces et Interfaces, DSM/DRECAM, Bâtiment 462, 91191 Gif-sur-Yvette, France

Received 20 March 2006, in final form 24 May 2006
Published 23 June 2006
Online at stacks.iop.org/JPhysCM/18/6307

Abstract

In this paper, we consider the problem of inelastic electron transport in molecular systems in which both electronic and vibrational degrees of freedom are considered on the quantum level. The electronic transport properties of the corresponding molecular nanojunctions are obtained by means of a non-perturbative Landauer-like multi-channel inelastic scattering technique. The connections between this approach and other Green's function techniques that are useful in particular cases are studied in detail. The validity of the wide-band approximation, the effects of the lead self-energy and the dynamical polaron shift are also studied for a wide range of parameters. As a practical application of the method, we consider the effects of the temperature on the conductance properties of molecular breakjunctions in relation to recent experiments.

1. Introduction

The electronic current-carrying ability of molecules is fundamental and important to a wide range of applications covering energy and information transfer to mono-molecular electronics [1–3]. It is now well established that the transport properties of single (or a few) molecules connected to external electrodes can be measured for a broad range of temperatures [1–3]. The transport properties have been measured for different kinds of molecules: linear organic conjugated molecules [4–8], carbon nanotubes [4, 9, 10], molecular complexes including metallic ions [11, 12], proteins and DNA-like sequences [13–15]. Very recently, the transport through single and substantially long ($\gg$100 Å) organic conjugated polymers has been measured at room temperature [16]. In contrast to conduction through macroscopic systems, new features appear in transport through molecules because of the different length and energy scales involved. It is known that the local interactions (interaction between electrons and/or interaction between electrons and atomic vibrations) play an important role in the transport properties [1–3]. The effects of these interactions are more

pronounced in nanoscale systems because the electronic probability density is concentrated in a smaller region of space, where normal screening mechanisms are modified and become less effective.

The effects of the interaction between electrons and molecular vibrations have been observed in recent experiments performed on molecular junctions [17–24]. On one hand, inelastic electron tunnelling spectroscopy (IETS) provides information about the selective excitation of specific vibration modes of the molecule itself or of the molecule/electrode interface as the electron is injected at a given energy (applied bias). IETS spectra have been measured for small molecules adsorbed on surfaces [17, 18], molecular-scale transistors [19], molecular nanojunctions made of alkyl or π-conjugated molecular wires [20], alkanedithiol monolayers [21] and dithiol benzene-based organic molecules taken as individual entities or embedded in a self-assembled monolayer [23]. On the other hand, the coupling between electron and molecular vibrations plays an important role in the transport properties of long conjugated molecules (conducting polymers) in which the transport is mediated via the propagation of complex objects such as polarons or solitons [24, 25].

There have been many theoretical investigations focusing on the effects of electron–vibration (or electron–phonon, e–ph) coupling in molecular and atomic scale wires. As far as the electronic transport properties are concerned, different approaches and different levels of approximations have been considered. Perturbation theory for the electron–vibration interaction has been used to interpret IETS spectra for model systems [26] and more realistic systems including small molecules on surfaces [27–29], atomic wires [30–32] and molecular wires [33–35]. Going beyond perturbative approximations, the effects of the e–ph coupling have been considered using scattering theory and conventional Green's function approaches [36–46], master and quantum kinetic equations [47], reduced electron-density matrix approaches [48], and non-adiabatic dynamics from lowest order expansions of the density matrix of the coupled electron–ion system [49]. Another model including dissipation within a semiclassical treatment of the atomic motion has also been developed [50]. More recently, approaches based on non-equilibrium statistical physics [51–54] have been used to study the effects of electron–vibration coupling in model systems [55–58] and in more realistic atomic and molecular wires [59–66].

In this paper, we present an alternative approach to treat exactly the coupling between an injected electron and either extended or localized molecular vibrations. In this approach, both fermionic and bosonic subsystems are treated on the quantum level. The transport properties of the corresponding molecular nanowires are obtained by means of a multi-channel inelastic scattering technique (section 2). The method is suited for both small and extended molecular systems. The basic principles of the multi-channel inelastic scattering technique are briefly described in section 2. The most important results are given in this section in order to show the connections between the multi-channel inelastic scattering technique and other methods that are useful in particular cases. The connection between the different approaches and the validity of the approximations used is discussed in section 3. Then in section 4 we show numerically how the energy dependence of the lead self-energy plays an important role in the transmission and we also study a special case for which artificial side-band peaks appear in the transmission. In section 4, we also study the dynamical effects of the polaron shift and we show the different regions of parameter space where the polaron shift effects may (or may not) be safely neglected. As a practical implementation of the technique, we consider in section 5 the effects of the temperature on the conductance properties for a model system in relation to recent experiments performed on conjugated molecular wires in breakjunctions [5]. Finally, we conclude and briefly discuss the future developments of the present work (section 6).

2. The physical model

The model involves the delocalized electronic states of the molecule which simultaneously carry current through the junction and interact with the eigenmodes of vibration of the molecule. In the case of conjugated molecules these states are predominantly derived from the π orbitals. However, the method can deal equally with other types of states, and there are no restrictions on the geometry or dimensionality of the problem. The reference Hamiltonian H_0 for the isolated molecule is

$$H_0 = H_{\rm el} + \sum_\lambda \omega_\lambda a_\lambda^\dagger a_\lambda \tag{1}$$

where $H_{\rm el}$ is the purely electronic Hamiltonian and λ labels the eigenmodes of vibration of the isolated molecule in its equilibrium (generally neutral) charge state; $a_\lambda^\dagger$ creates (a_λ annihilates) a quantum of energy ω_λ in mode λ. The molecular vibrations are assumed to be approximately harmonic. The electronic Hamiltonian $H_{\rm el}$ may, in principle, contain electron–electron interactions.

The fundamental approximation in the following is to consider the scattering of *single* electrons or holes from the molecule. This assumption is expected to be reasonable when the interval between carrier transmission events is much greater than the transit time through the molecule [41], and when the applied bias does not cause significant fluctuations in the occupancy of the molecular eigenstates (i.e. one charge state of the molecule dominates during the transport process).

For electron transport, if the equilibrium charge state contains N electrons and $|0, N\rangle$ is the N-electron ground state, we construct an electronic basis $|i, N+1\rangle = c_i^\dagger |0, N\rangle$ where the $\{c_i^\dagger\}$ create an electron in a sufficiently complete set of orbitals (for example, in all the low-lying π-states of the molecule). For hole transport, we would use $|j, N-1\rangle = c_j|0, N\rangle$. The electron Hamiltonian $H_{\rm el}$ is then diagonalized (keeping the phonon coordinates fixed, for the moment) within the restricted $(N \pm 1)$-electron basis to obtain a set of approximate $(N \pm 1)$-electron eigenstates. Using the corresponding electron creation ($c_n^\dagger$) and annihilation (c_n) operators and the energies ϵ_n, we can write

$$H_{\rm el} = \sum_n \epsilon_n c_n^\dagger c_n. \tag{2}$$

The approximate $(N \pm 1)$-electron eigenstates of the full H_0 can thus be written as a direct product of the electronic states and the vibrational states, $|n, \{n_\lambda\}\rangle = |n\rangle \otimes |\{n_\lambda\}\rangle$, where n labels an electronic eigenstate and the $\{n_\lambda\}$ are occupation numbers for the vibrational modes:

$$|n, \{n_\lambda\}\rangle = c_n^\dagger \prod_\lambda \frac{(a_\lambda^\dagger)^{n_\lambda}}{\sqrt{n_\lambda!}} |0, N\rangle \otimes |\{0_\lambda\}\rangle \tag{3}$$

for electrons, with an obvious generalization for holes.

The e–ph coupling term $H_{\rm eph}$ is taken to be linear in the phonon displacements and induces transitions between the electronic states:

$$H_{\rm eph} = \sum_{\lambda,n,m} \gamma_{\lambda nm} (a_\lambda^\dagger + a_\lambda) c_n^\dagger c_m. \tag{4}$$

The derivation of equation (4) from a linearized tight-binding model of a *trans*-polyacetylene chain (the Su–Schrieffer–Heeger model [25]) can be found in [41]. However, the values of ϵ_n, ω_λ needed in H_0 and of $\gamma_{\lambda nm}$ needed in $H_{\rm eph}$ can be taken from any suitable model of the molecule (i.e. an isolated molecule or a molecule in contact with clusters representing a part of the junction).

To obtain the transport properties, the molecule is connected to two metallic (left L and right R) leads. As mentioned above, we consider the scattering of a single incoming charge carrier (electron or hole). The coupling matrix elements between the molecule and the leads are $v_{\mathrm{L,R}}$ respectively. Since we do not wish to focus only on the properties of the leads, the simplest possible model is considered, i.e. one-dimensional semi-infinite chains with on-site energy $\epsilon_{\mathrm{L,R}}$ and hopping integrals $\beta_{\mathrm{L,R}}$ between nearest neighbours. However, a generalization to a more realistic coupling of the molecule to the leads is straightforward. In the next section, we will show results obtained for different models for the leads which go beyond the one-dimensional semi-infinite chain.

The transport is assumed to be purely elastic within the leads themselves; dissipation of hot electrons occurs only in remote reservoirs, as in the standard Landauer picture for electron transport. The scattering states $|\Psi\rangle$ for a single incoming carrier are then expanded inside the molecule onto the eigenstates $|n, \{n_\lambda\}\rangle$ of H_0. The single added carrier can be anywhere in the system and interacts with lattice vibrations only when inside the molecule. The problem is then solved by mapping the many-body problem onto a single-electron one with many scattering channels [37–39, 41]; each channel represents a process by which the electron might exchange energy with the vibration modes.

For an initial vibration mode distribution $b \equiv \{m_\lambda\}$ before scattering and an incoming electron from the left, the outgoing channels in the left and right leads are associated with energy-dependent reflection coefficients r_{ab} and transmission coefficients t_{ab}, where $a \equiv \{n_\lambda\}$ is the final mode distribution after scattering. In the leads, the scattering states are propagating waves with amplitudes r_{ab} (reflection) and t_{ab} (transmission), and wavevectors k_b^{L} and $k_a^{\mathrm{L,R}}$ corresponding to the initial (ϵ_{in}) and final (ϵ_{fin}) electronic energies. By projecting out the leads, one works in the molecular subspace to obtain the scattering state $|\Psi\rangle$ by solving

$$\left[\omega - H_0 - H_{\mathrm{eph}} - \Sigma_{\mathrm{L}}^{\mathrm{r}}(\omega) - \Sigma_{\mathrm{R}}^{\mathrm{r}}(\omega)\right]|\Psi(\omega)\rangle \equiv G^{\mathrm{r}}(\omega)^{-1}|\Psi(\omega)\rangle = |s_b(\omega)\rangle. \tag{5}$$

Here ω is the conserved total energy:

$$\omega = \epsilon_{\mathrm{in}} + \sum_\lambda m_\lambda \omega_\lambda = \epsilon_{\mathrm{fin}} + \sum_\lambda n_\lambda \omega_\lambda. \tag{6}$$

The source term $|s_b(\omega)\rangle$ is fixed by the incoming boundary conditions, while $\Sigma_{\mathrm{L,R}}^{\mathrm{r}}(\omega)$ are the electron self-energies arising from the coupling of the molecule to the leads [41]. Note that since the lead properties appear in the form of a self-energy, it is easy to introduce any more realistic model for the contacts and the electrodes via these self-energies.

The components of the scattering states $|\Psi\rangle$ give the matrix elements of the retarded Green's function G^{r}. In practice, the linear system $|\Psi\rangle = G^{\mathrm{r}}|s\rangle$ is solved for a finite-size molecular subspace, by truncating the occupation number above a maximum $n_\lambda^{\max}$ in each mode. This is physically reasonable because the injected charge cannot populate infinitely many excitations. From the solution of equation (5), the expectation value of an operator A is calculated as

$$\langle A\rangle = \sum_b \mathcal{W}_b^{\mathrm{ph}}(T)\langle\Psi|A|\Psi\rangle, \tag{7}$$

where $\mathcal{W}_b^{\mathrm{ph}}(T)$ is the statistical weight of the initial distribution $b \equiv \{m_\lambda\}$ of vibration modes λ at temperature T.

The transmission probability $T_{ab}(\omega)$ is given from the square of the coefficients t_{ab} with the usual ratio of the electron velocities in the outgoing and incoming channels. In our model, the transmission probability T_{ab} is obtained as [36, 41–44]

$$T_{ab}(\epsilon_{\mathrm{fin}}, \epsilon_{\mathrm{in}}) = 4\,\frac{v_{\mathrm{L}}^2}{\beta_{\mathrm{L}}}\sin k_b^{\mathrm{L}}(\epsilon_{\mathrm{in}})\frac{v_{\mathrm{R}}^2}{\beta_{\mathrm{R}}}\sin k_a^{R}(\epsilon_{\mathrm{fin}})|\langle i = N|G_{ab}^{\mathrm{r}}(\omega)|i = 1\rangle|^2, \tag{8}$$

where $\langle N|G^{\rm r}_{ab}(\omega)|1\rangle$ is the matrix element of the Green's function $G^{\rm r}$ taken between the left side ($i = 1$) and the right side ($i = N$) of the molecule and the vibration distributions before (b) and after (a) scattering. The factors $\Gamma_{\rm L,R}(\omega) = 2v^2_{\rm L,R}/\beta_{\rm L,R}\sin k^{\rm L,R}_{b,a}(\omega)$ are related to the imaginary parts of the retarded self-energies $\Sigma^{\rm r}_{\rm L,R}$.

It is interesting to note that the sum of the different contributions $\sum_{a,b}\mathcal{W}^{\rm ph}_b(T)T_{ab}$ is related to the expression of the generalized transmission $\mathrm{Tr}[\Gamma_{\rm L}G^{\rm a}\Gamma_{\rm R}G^{\rm r}]$ which is usually derived for non-interacting systems. The derivation of a Landauer-like inelastic transmission for interacting systems has been recently given in [67], where it is argued that the Landauer picture is still valid in the presence of interaction as long as multi-particle processes can be neglected.

Finally, two important notes are in order. First, the procedure described above solves the problem *non-perturbatively* in the e–ph interaction. Second, the method has been described for the case where the channel structure of the leads is generated only by the vibrational excitations of the molecule. It is however straightforward to generalize it to the cases of multiple spatial channels in the leads.

3. Connection to other approaches: transmission versus Green's functions

In this section, we show analytically how the multi-channel scattering technique described in the previous section is related to other Green's function methods. The most important results are given in the following subsections while, for clarity, we have compiled the detailed derivations in the appendices.

We also introduce further simplifications, which permit us to keep a simple formalism without losing its generality or affecting the main physical results.

3.1. The single-particle approximation

Let us first assume that the left and right leads are identical and that the molecule's ends are coupled to the leads via energy-independent hopping integrals. Then, the self-energies $\Sigma^{\rm r}_{\rm R}(\omega)$ and $\Sigma^{\rm r}_{\rm L}(\omega)$ (and their imaginary parts $\Gamma_{\rm L,R}$) are proportional to each other. The current through the molecular junction is given by (see appendix A)

$$J = -\frac{2e}{h}\int \mathrm{d}\omega\,(f_{\rm L}(\omega) - f_{\rm R}(\omega))\,\mathrm{Im}\,\mathrm{Tr}\{\Gamma(\omega)G^{\rm r}(\omega)\}, \tag{9}$$

where $f_{\rm L,R}$ is the Fermi distribution of the left and right lead respectively, $G^{\rm r}$ is the retarded Green's function of the molecule and $\Gamma = \Gamma_{\rm L}\Gamma_{\rm R}/(\Gamma_{\rm L} + \Gamma_{\rm R})$. $G^{\rm r}$ includes the self-energies arising from the coupling to the leads and from the e–ph interaction.

Let us further assume that the molecular Hamiltonian $H = H_0 + H_{\rm eph}$ is simplified to one electronic level ϵ_0 coupled to a single vibration mode of frequency ω_0 via a coupling constant γ_0 (i.e. the single-site–single-mode SSSM model). The SSSM Hamiltonian is then

$$H = H_0 + H_{\rm eph} = \epsilon_0 c^\dagger_0 c_0 + \omega_0 a^\dagger_0 a_0 + \gamma_0(a^\dagger_0 + a_0)c^\dagger_0 c_0. \tag{10}$$

Within the SSSM model, the trace in equation (9) runs over the vibration harmonic states $|\chi_n\rangle$ associated with the creation $a^\dagger_0$ (annihilation a_0) operator of the vibration mode ω_0:

$$\mathrm{Tr}\{\Gamma(\omega)G^{\rm r}(\omega)\} = \sum_n \mathcal{W}^{\rm ph}_n(T)\langle\chi_n|\Gamma G^{\rm r}|\chi_n\rangle, \tag{11}$$

where the phonon statistical weight is given by $\mathcal{W}^{\rm ph}_n(T) = (1 - \mathrm{e}^{-\omega_0/kT})\mathrm{e}^{-n\omega_0/kT}$.

When the e–ph coupling occurs only inside the molecule, Γ conserves the phonon energy and occupation, and

$$\mathrm{Tr}\{\Gamma G^{\mathrm{r}}\} = \sum_n \mathcal{W}_n^{\mathrm{ph}}(T)\langle\chi_n|\Gamma|\chi_n\rangle\langle\chi_n|G^{\mathrm{r}}|\chi_n\rangle. \tag{12}$$

In the limit of low temperatures ($\omega_0 \ll kT$), the properties are determined only by the phonon ground-state $|\chi_0\rangle$ ($\mathcal{W}_n^{\mathrm{ph}} = 0$ for $n > 0$) and $\mathrm{Tr}\{\Gamma G^{\mathrm{r}}\} = \Gamma(\omega)\langle\chi_0|G^{\mathrm{r}}(\omega)|\chi_0\rangle$.[1]

Furthermore, within the SSSM model, G^{r} is the inverse of a tridiagonal matrix R in the subspace of the harmonic vibrational states $|\chi_n\rangle$ with non-zero matrix elements:

$$R_{n,n} = \omega - \epsilon_0 - n\omega_0 - \Sigma^{\mathrm{r}}_{\{n\}}, \qquad R_{n,n+1} = -\sqrt{n+1}\,\gamma_0, \qquad R_{n,n-1} = -\sqrt{n}\,\gamma_0. \tag{13}$$

$\Sigma_{\{n\}}(\omega)$ is the self-energy arising from the coupling to both left and right leads. The index n corresponds to a different transport channel containing n excitations of the vibration mode. $\Sigma_{\{n\}}$ is calculated by taking into account the conserved-energy relation equation (6) and has the following property [41]: $\Sigma_{\{n\}}(\omega) = \Sigma_{\{0\}}(\omega - n\omega_0)$.

In the limit of low temperatures, the conserved-energy relation equation (6) reduces to $\omega = \epsilon_{\mathrm{in}} = \epsilon_{\mathrm{fin}} + n\omega_0$ and the only important matrix element $G^{\mathrm{r}}_{00} = \langle\chi_0|G^{\mathrm{r}}|\chi_0\rangle$ can be written as a continued fraction:

$$G^{\mathrm{r}}_{00}(\omega) = \left[\omega - \epsilon_0 - \Sigma^{\mathrm{r}}_{\{0\}} - \cfrac{\gamma_0^2}{\omega - \epsilon_0 - \omega_0 - \Sigma^{\mathrm{r}}_{\{1\}} - \cfrac{2\gamma_0^2}{\omega - \epsilon_0 - 2\omega_0 - \Sigma^{\mathrm{r}}_{\{2\}} - \frac{3\gamma_0^2}{\omega - \epsilon_0 - 3\omega_0 - \Sigma^{\mathrm{r}}_{\{3\}} - \cdots}}}\right]^{-1}. \tag{14}$$

The imaginary part of G^{r}_{00} is obtained from the sum of different terms:

$$\mathrm{Im}\, G^{\mathrm{r}}_{00}(\omega) = |G^{\mathrm{r}}_{00}(\omega)|^2\, \mathrm{Im}\left\{\Sigma_{\{0\}}(\omega) + \frac{\gamma_0^2}{\omega - \epsilon_0 - \omega_0 - \Sigma^{\mathrm{r}}_{\{1\}}(\omega) - \cdots}\right\}. \tag{15}$$

It can be shown that the imaginary part of G^{r}_{00} is in fact related to the other non-diagonal elements $\langle\chi_n|G^{\mathrm{r}}|\chi_0\rangle$ of G^{r} in the following manner:

$$\begin{aligned}\mathrm{Im}\langle\chi_0|G^{\mathrm{r}}|\chi_0\rangle = {} & \mathrm{Im}\,\Sigma^{\mathrm{r}}_{\{0\}}\,|\langle\chi_0|G^{\mathrm{r}}|\chi_0\rangle|^2 + \mathrm{Im}\,\Sigma^{\mathrm{r}}_{\{1\}}\,|\langle\chi_1|G^{\mathrm{r}}|\chi_0\rangle|^2 \\ & + \mathrm{Im}\,\Sigma^{\mathrm{r}}_{\{2\}}|\langle\chi_2|G^{\mathrm{r}}|\chi_0\rangle|^2 + \cdots.\end{aligned} \tag{16}$$

This is an important result which allows us to relate Green's function approaches to Landauer-like transmission approaches. Indeed, by introducing equation (16) in the current formula equation (9), the current J is then obtained as the sum of the elastic $T_{bb}(\epsilon, \epsilon)$ and inelastic $T_{ab}(\epsilon', \epsilon)$ transmission probabilities defined in section 2. The transmissions T_{ab} are given by equation (8) and evaluated for the SSSM model where the vibration is initially in the ground state ($b \equiv |\chi_0\rangle$) and in the nth excited state ($a \equiv |\chi_n\rangle$) after scattering. The detailed derivation of the series expansion of the current in terms of transmission is given at the end of appendix A. A similar series expansion of the current has also recently been obtained by a Landauer-like approach for interacting systems [67].

[1] In terms of scattering, the vibration mode is initially in the nth (excited) state and the injected electron scatters out elastically in the same nth channel and inelastically in the $(n+m)$th channel by emission of m phonons and in the $(n-m)$th channel by phonon absorption. At zero temperature only the term $n = 0$ matters and only phonon emission processes are available.

For finite temperature T, the current is calculated from all the diagonal elements $\langle\chi_n|G^{\rm r}|\chi_n\rangle$ with the appropriate statistical weight $\mathcal{W}_n^{\rm ph}(T)$ for the nth excitation of the vibration mode. Each matrix element $\langle\chi_n|\Gamma|\chi_n\rangle\,{\rm Im}\langle\chi_n|G^{\rm r}|\chi_n\rangle$ is then related to the sum over $a \equiv |\chi_m\rangle$ of the transmission coefficients T_{ab}. Another series expansion of the current is obtained as described above. However, here one starts with different initial thermal distributions $b \equiv |\chi_n\rangle$ of the vibration.

Finally, let us note that although the connection between the multi-channel scattering technique and conventional Green's function approach has been demonstrated only for the SSSM model, it can be generalized to the cases of many electronic levels coupled to many vibration modes, equations (1)–(4). In these cases, the matrix R which defines $G^{\rm r}$ is tridiagonal by blocks (the diagonal blocks being associated with the different electronic levels and phonon replica, the off-diagonal with the e–ph coupling matrix $\gamma_{\lambda nm}$). The matrix element $\langle\{0_\lambda\}|G^{\rm r}|\{0_\lambda\}\rangle$ equivalent to equation (14) can then be written as a matrix continued fraction in the corresponding subspace. The same reasoning as above can be applied to the derivation of the current in terms of elastic and inelastic transmission probabilities T_{ab} for all temperatures.

3.2. The wide-band approximation

In this section, we show how the multi-channel scattering technique is related to the work of Wingreen *et al* [68] via equation (16). For this, we consider the wide-band approximation for the leads. For the energy range considered, the lead densities of states are relatively flat and featureless and the lead self-energies become independent of the energy and of the transport channel: $\Sigma_{\{n\}}(\omega) \equiv -{\rm i}\Gamma = -{\rm i}(\Gamma_{\rm L}+\Gamma_{\rm R})/2$ with $\Gamma > 0$. It is sometimes convenient to consider such an approximation because it simplifies the subtleties of parameter renormalization which appear when one introduces the unitary transformation $U = \exp g(a_0 - a_0^\dagger)$ with $g = \gamma_0/\omega_0$ that diagonalizes the SSSM Hamiltonian (see appendix B and discussion therein).

By applying the unitary transformation U to the SSSM Hamiltonian, $G^{\rm r}$ is the inverse of the diagonal matrix $R_{l,l} = \omega - (\epsilon_0 - g^2\omega_0) - l\omega_0 + {\rm i}\Gamma$ within the space of the basis set $|\tilde\chi_n\rangle = U|\chi_n\rangle$ corresponding to the harmonic states of the displaced vibration mode.

In the wide-band approximation, the imaginary part of $G^{\rm r}_{00}$ in equation (16) simply becomes ${\rm Im}\,G^{\rm r}_{00}(\omega) = \sum_n -\Gamma|\langle\chi_n|G^{\rm r}|\chi_0\rangle|^2$. By introducing the basis set $|\tilde\chi_n\rangle$, one gets

$$
{\rm Im}\,G^{\rm r}_{00}(\omega) = -\Gamma\sum_n\left|\sum_l\langle\chi_n|\tilde\chi_l\rangle\frac{1}{\omega-(\epsilon_0-g^2\omega_0)-l\omega_0+{\rm i}\Gamma}\langle\tilde\chi_l|\chi_0\rangle\right|^2. \tag{17}
$$

Using the expressions for the overlaps between the harmonic states $|\chi_n\rangle$ and the displaced harmonic states $|\tilde\chi_n\rangle$, one finds that (see appendix B)

$$
\begin{aligned}
{\rm Im}\,G^{\rm r}_{00}(\omega) = -\Gamma{\rm e}^{-2g^2}\sum_{n=0}^{\infty}\frac{g^{2n}}{n!}\Bigg|\sum_{j=0}^{n}(-1)^j \\
\times\binom{n}{j}\sum_{l=0}^{\infty}\frac{g^{2l}}{l!}\frac{1}{\omega-(\epsilon_0-g^2\omega_0)-(j+l)\omega_0+{\rm i}\Gamma}\Bigg|^2.
\end{aligned} \tag{18}
$$

Equation (18) is the same result as obtained by Wingreen *et al* in [68] where the authors derived the effective transmission from a two-particle Green's function approach for a single electronic level coupled to a single vibration mode.

3.3. The non-equilibrium Green's function approaches

In this section, we show the relationship between the multi-channel scattering technique and other approaches based on non-equilibrium Green's functions [54, 56, 57, 59, 61, 62].

First of all, the retarded Green's function G^{r} given in equation (14) can be rewritten in a more compact form:

$$G^{\mathrm{r}}(\omega) = [\, g_0^{\mathrm{r}}(\omega)^{-1} - \Sigma^{\mathrm{r}}_{\mathrm{leads}}(\omega) - \Sigma^{\mathrm{r}}_{\mathrm{eph}}(\omega)]^{-1}. \tag{19}$$

In this expression G^{r} includes the retarded self-energies arising from the coupling of the molecule to the leads ($\Sigma^{\mathrm{r}}_{\mathrm{leads}} = \Sigma^{\mathrm{r}}_{\{0\}}$) and from the interaction between the electron and the vibration ($\Sigma^{\mathrm{r}}_{\mathrm{eph}}$), and g_0^{r} is the retarded Green's function of the isolated molecule in the absence of e–ph coupling.

To the lowest order in the e–ph coupling, the self-energy $\Sigma^{\mathrm{r}}_{\mathrm{eph}}$ is given by $\Sigma^{\mathrm{r},(1)}_{\mathrm{eph}}(\omega) = \gamma_0^2 G^{\mathrm{r}}(\omega - \omega_0)$. The detailed derivation and the discussion of such a result is given in appendix C. Now we show how this result is related to non-equilibrium Green's function techniques.

In a many-body non-equilibrium approach, the self-energies arising from the interaction between particles are obtained from a diagrammatic perturbation expansion of the interaction and by applying the rules for the time ordering and for the evaluation of products of double-timed operators on the Keldysh contour [52].

For a coupled e–ph system, one should in principle take into account all processes to all orders of the interaction to calculate self-consistently the different electron Green's functions dressed by the phonons as well as the different phonon Green's functions dressed by the electrons. This is a tremendous task to achieve for realistic systems, and it has been done almost exactly only for model systems and within some approximations for atomic or molecular wires. Recent studies based on such non-equilibrium many-body techniques have been performed by using the so-called self-consistent Born approximation [57, 59, 61, 62]. Within this approximation, the retarded electron self-energy due to the e–ph coupling is obtained as a sum of three contributions $\Sigma^{\mathrm{r}}_{\mathrm{eph}} = \Sigma^{\mathrm{r}}_{\mathrm{eph,rr}} + \Sigma^{\mathrm{r}}_{\mathrm{eph},>\mathrm{r}} + \Sigma^{\mathrm{r}}_{\mathrm{eph,r}>}$ where each contribution has the following functional form:

$$\Sigma^{\mathrm{r}}_{\mathrm{eph},XY}(\omega) = \pm \mathrm{i}\, \gamma_0^2 \int \frac{\mathrm{d}\omega'}{2\pi} D^X(\omega - \omega')\, G^Y(\omega'). \tag{20}$$

The sub/superscript X, Y represents a different kind (retarded r, greater $>$) of Green's functions for electrons (G^Y) and phonons (D^X).

We now analyse how these contributions are related to the self-energy $\Sigma^{\mathrm{r},(1)}_{\mathrm{eph}}$ derived in appendix C. For this, we consider that the phonon Green's functions are given by the undressed phonon propagator $D_0(\omega)$ for which the Keldysh greater component is

$$D_0^{>}(\omega) = -\mathrm{i}2\pi(N(\omega)\delta(\omega + \omega_0) + (N(\omega) + 1)\,\delta(\omega - \omega_0)), \tag{21}$$

$N(\omega)$ being the Bose–Einstein distribution function for the vibration mode at temperature T (within the SSSM model, $N(\omega_0) = \sum_n n\mathcal{W}_n^{\mathrm{ph}}(T)$). Furthermore, we concentrate on the limit of low temperatures for which simplifications arise because then $N(\omega) = 0$.

By using the principle of causality and the analytic properties of G^{r} in the complex plane, it can be shown that the contribution

$$\Sigma^{\mathrm{r}}_{\mathrm{eph,rr}}(\omega) = -\mathrm{i}\gamma_0^2 \int \frac{\mathrm{d}\omega'}{2\pi} D_0^{\mathrm{r}}(\omega - \omega')\, G^{\mathrm{r}}(\omega') \tag{22}$$

to the e–ph self-energy vanishes[2]. The second contribution to the self-energy is

$$\Sigma^{\mathrm{r}}_{\mathrm{eph},>\mathrm{r}}(\omega) = \mathrm{i}\gamma_0^2 \int \frac{\mathrm{d}\omega'}{2\pi} D_0^{>}(\omega - \omega')\, G^{\mathrm{r}}(\omega'). \tag{23}$$

[2] This is true for systems with electron–hole symmetry and also for the other cases when the systems are not too far from equilibrium.

At zero temperature, this self-energy is exactly the self-energy $\Sigma^{\mathrm{r},(1)}_{\mathrm{eph}} = \gamma_0^2 G^{\mathrm{r}}(\omega-\omega_0)$ derived in appendix C for the lowest order in the e–ph coupling.

The last contribution to the self-energy is

$$\Sigma^{\mathrm{r}}_{\mathrm{eph,r}>}(\omega) = \mathrm{i}\gamma_0^2 \int \frac{\mathrm{d}\omega'}{2\pi}(D^{\mathrm{r}}_0(\omega') - D^{\mathrm{r}}_0(\omega=0))G^{>}(\omega-\omega'). \tag{24}$$

It involves the greater electron Green's function $G^{>}$ which provides information about the non-equilibrium density of unoccupied states of the molecule. These states become partially filled when the current flows through the molecule. $G^{>}$ is related to the corresponding self-energy $\Sigma^{>} = \Sigma^{>}_{\mathrm{L}} + \Sigma^{>}_{\mathrm{R}} + \Sigma^{>}_{\mathrm{eph}}$ and to the retarded and advanced Green's functions $G^{\mathrm{r,a}}$ via the kinetic equation $G^{>}(\omega) = G^{\mathrm{r}}(\omega)\Sigma^{>}(\omega)G^{\mathrm{a}}(\omega)$. Without entering into a lengthy explanation, the terms in equation (24) involving $\Sigma^{>}_{\mathrm{eph}}$ in $G^{>}$ are intrinsically of higher order in $\mathcal{O}[\gamma_0^2]$ than $\Sigma^{\mathrm{r},(1)}_{\mathrm{eph}}$. They become negligible for weak e–ph coupling. The other terms involving $\Sigma^{>}_{\mathrm{L,R}}$ in $G^{>}$ are important. However, their contributions are small when the electronic level coupled to the vibration is off-resonance with the Fermi levels of the leads (in the limit of zero to small applied bias). This is usually the case for molecules having a substantial HOMO–LUMO gap and when the leads' Fermi levels are pinned inside this gap.

All the different non-equilibrium contributions to the e–ph self-energies are not yet properly included in the present form of the multichannel scattering technique. However, one of them ($\Sigma^{\mathrm{r}}_{\mathrm{eph},>\mathrm{r}}$) is already included and to a higher order in $\mathcal{O}[\gamma_0^2]$ than the self-energy $\Sigma^{\mathrm{r},(1)}_{\mathrm{eph}}$ obtained from the self-consistent Born approximation. This is very important when polaronic effects dominate the transport properties (see appendix C). Furthermore, as mentioned above, the other contributions ($\Sigma^{\mathrm{r}}_{\mathrm{eph,r}>}$ and $\Sigma^{\mathrm{r}}_{\mathrm{eph,rr}}$) are negligible in the limit of non-resonant transport and not too far from equilibrium.

4. Transmission versus lead self-energy and dynamical polaron shift

Now that we have shown analytically how the multi-channel scattering technique is related to other Green's function approaches, we present numerical calculations for the different models derived in sections 2, 3.1 and 3.2. In particular, we show how different models for the lead self-energy (wide-band approximation or energy dependent self-energy) affect the transmission. We also study an important physical effect which is neglected in the wide-band approximation, namely the dynamical polaron shift. We also show the different regions of parameter space where the polaron shift is important or not.

4.1. The dependence of the transmission on the lead self-energy

Figure 1 shows the effective transmission $T_{\mathrm{eff}}(\omega) = -\Gamma(\omega)\,\mathrm{Im}\,G^{\mathrm{r}}_{00}(\omega)$ obtained for the different models studied in the previous section. The different corresponding expressions for $G^{\mathrm{r}}_{00}(\omega)$ are given by equations (14), (18) and (B.10). The upper part of figure 1 shows, as expected, that in the wide-band approximation the transmissions obtained from equations (18) and (B.10) are strictly equivalent. However, the transmission calculated from equation (14) is different because it takes into account the energy dependence of the lead self-energy. One obtains small shifts in the transmission peaks because $\mathrm{Re}\,\Sigma^{\mathrm{r}}_{\{n\}}(\omega) \neq 0$ in equation (14), in contrast to the wide-band approximation, and the transmission is reduced at high energies because $\mathrm{Im}\,\Sigma^{\mathrm{r}}_{\{n\}}(\omega)$ has a finite energy support; i.e., for large ω or large n, one has $\mathrm{Im}\,\Sigma^{\mathrm{r}}_{\{n\}}(\omega) = \mathrm{Im}\,\Sigma^{\mathrm{r}}_{\{0\}}(\omega - n\omega_0) = 0$.

Furthermore, the overall shape of the transmission is strongly dependent on the model taken for the self-energy $\Sigma^{\mathrm{r}}_{\{n\}}(\omega)$ (i.e. for the leads and their contacts to the molecule). The

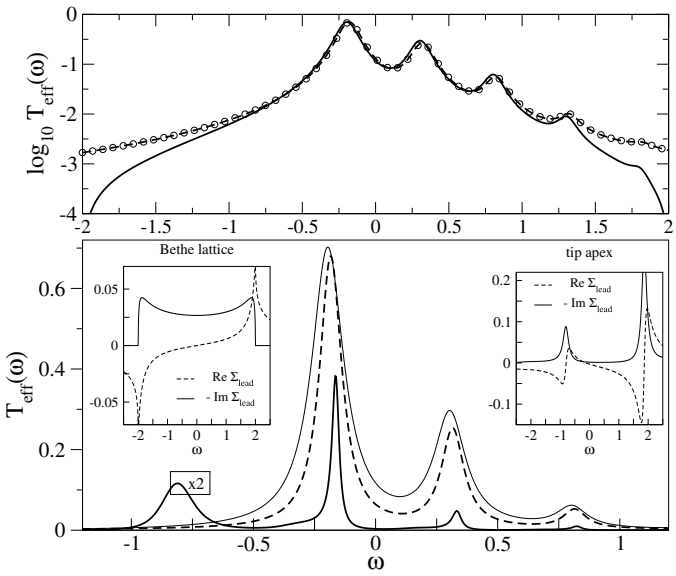

Figure 1. Effective transmission $T_{\rm eff}(\omega) = -\Gamma(\omega)\,{\rm Im}\,G^{\rm r}_{00}(\omega)$ calculated for the SSSM model. *Upper panel*, ${\rm Im}\,G^{\rm r}_{00}(\omega)$ obtained from equation (14) (*solid line*), from equation (18) (*dashed line*), from equation (B.10) (○). For the *solid line*, the lead self-energy $\Sigma^{\rm r}_{\{0\}}(\omega)$ is shown in the inset of figure C.1. For the wide-band approximation (*dashed line* and ○), one takes $\Gamma = {\rm Im}\,\Sigma^{\rm r}_{\{0\}}(\omega = 0)$. *Lower panel*, $T_{\rm eff}$ for different models of leads: *thin solid line*, model (i) with $\Sigma^{\rm r}_{\{0\}}$ shown in the inset of figure C.1; *dashed line*, model (ii) with $\Sigma^{\rm r}_{\{0\}}$ shown in the lower left inset; *solid line*, model (ii) with $\Sigma^{\rm r}_{\{0\}}$ shown in the lower right inset (the magnitude of $T_{\rm eff}$ is $\times 2$). The other parameters are $\epsilon_0 = 0$, $\omega_0 = 0.5$, $\gamma_0 = 0.3$ and $v = 0.2$ with $v_{\rm L,R} = v$ and $\beta_{\rm L,R} = \beta = 1$.

lower part of figure 1 shows how the features in the transmission are modified by considering different models for the leads. These models are (i) a semi-infinite tight-binding chain whose corresponding semi-elliptic surface local density of states generates the self-energy $\Sigma^{\rm r}_{\{0\}}(\omega)$ shown in the inset of figure C.1, (ii) a Bethe lattice with coordination three (the corresponding $\Sigma^{\rm r}_{\{0\}}$ is shown in the lower left inset in figure 1) and (iii) a supported pyramidal tip made of transition metals [69, 70], whose corresponding self-energy is shown in the lower right inset in figure 1.

When the leads' surface density of states is relatively featureless (i.e. for models (i) and (ii)), the overall shape of the corresponding transmission is mostly conserved. There are however small differences in the exact position, width and height of the transmission peaks (see lower panel of figure 1). These differences arise from the different energy behaviour of the real and imaginary parts of $\Sigma^{\rm r}_{\{0\}}$ for the different models.

However, when the surface density of states of the leads presents sharp features as obtained for model (iii) (see imaginary part of $\Sigma^{\rm r}_{\{0\}}$ in the lower right inset of figure 1), one obtains new peaks in the transmission. These new peaks do not correspond to spectral features of the molecule itself. They are solely related to the spectral densities of the leads. Model (iii) might be an extreme pathological case; however, it shows that, in some energy range, the transmission conveys only information about the contacts spectral densities. This important result proves once more that the transport properties of molecular junctions depend not only on the molecule itself but also (and strongly in some cases) on the contacts between the molecule and the leads. These effects (contact geometry, dimensionality) have also been considered in other studies on model systems [71] and on more realistic molecular wires [72] and carbon nanotubes [73].

Now that we have shown how the transmission depends on the lead self-energies, we focus on another very important physical effect: the dynamical polaron shift.

4.2. The dynamical polaron shift

When the molecule is charged (permanently or temporarily), the vibration modes reorganize to accommodate the charge (electron or hole) because charge and vibrations are coupled together. The polaron shift corresponds to the shift of the nominal electronic levels due to this reorganization. Obviously any shift of the electronic levels will affect the value of the transmission at a given energy.

One can already distinguish two limiting cases for the value of the polaron shift. On one hand, there is no polaron shift in the absence of e–ph coupling and in the limit of extremely weak e–ph coupling. On the other hand, the full polaron shift is only obtained for a fully and permanently charged molecule (an isolated molecule) or within the wide-band approximation [68, 74, 75]. In all the other cases, the energy dependence of the lead self-energies $\Sigma^{\mathrm{r}}_{\{n\}}(\omega)$ plays an important role in the value of the polaron shift since the imaginary part of $\Sigma^{\mathrm{r}}_{\{n\}}$ is related to the escape rate of the electron from the molecule to the leads. In other words, when the residence time of the electron in the molecule [41, 76] is not long enough for the vibrations to fully respond to the presence of this electron, the full relaxation of the molecule is not obtained and one gets an intermediate value of the polaron shift.

Within the SSSM model, the full polaron shift is given by $E_{\mathrm{p}}^0 = -\gamma_0^2/\omega_0$, and for the wide-band approximation the nominal electronic level ϵ_0 is lowered by E_{p}^0 (see appendix B). For an energy-dependent lead self-energy, the dynamical polaron shift E_{p} is shown in figure 2 for different regions of the parameter space. The dynamical polaron shift E_{p} is calculated as the energy difference between the position of the lowest energy peak in the total effective transmission $T_{\mathrm{eff}}(\omega)$ and ϵ_0.

For weak coupling $v = v_{\mathrm{L}} = v_{\mathrm{R}}$ of the molecule to the leads (approximately when $v^2 < \omega_0/4$), the injected electron stays long enough in the molecule to obtain the full polaron shift $E_{\mathrm{p}} \sim E_{\mathrm{p}}^0$. For increasing values of v from weak to strong coupling, the electron residence time decreases and the vibration frequency might be not large enough to fully respond to the presence of the electron. One then observes an intermediate polaron shift $|E_{\mathrm{p}}| < |E_{\mathrm{p}}^0|$ with E_{p} being still proportional to E_{p}^0 (see the left panel in figure 2). For strong e–ph coupling and strong coupling to the leads, E_{p} is no longer proportional to E_{p}^0 (see the left panel in figure 2). For strong coupling to the leads and for a broad range of e–ph coupling (weak, medium to strong), the polaron shift has almost vanished when $v^2 > 3\beta\omega_0$ (see the right panel in figure 2). It is also interesting to note that an approximate scaling law $E_{\mathrm{p}}/E_{\mathrm{p}}^0 \sim f(v/\sqrt{\beta\omega_0})$ is obtained for the different regimes considered (i.e. weak to strong e–ph coupling within the adiabatic or non-adiabatic limit).

The results in figure 2 show the regions of the parameter space where the polaron shift effect should not be neglected (for example, when the coupling to the leads is weak, or for large vibration frequencies, it is valid to only consider the full polaron shift [68, 74, 75]) and the regions where the polaron shift can be safely neglected as in [77]. The effect of the polaron shift on the transmission might be not too important for quasi-ballistic atomic-size wires or metallic carbon nanotubes. However, it is very important for semiconducting-like wires, in which the polaron shift of the electronic-band-edge states can significantly reduce the energy gap of the system [38, 41].

Finally, to conclude this section, it should be noticed that such dynamical polaron shift effects cannot be obtained at all from any perturbation treatments of the e–ph coupling [78].

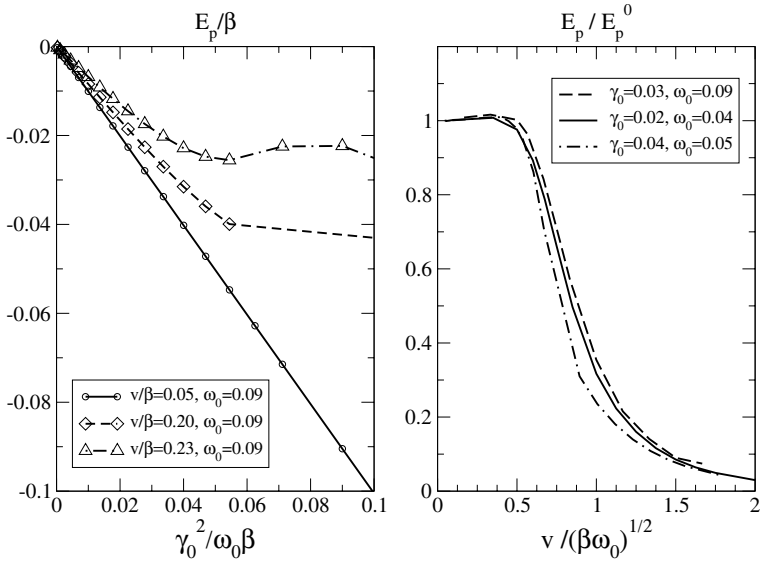

Figure 2. Dynamical polaron shift E_p for different parameter ranges. E_p is calculated as the difference between ϵ_0 and the position of the lowest energy peak in $T_{\rm eff}(\omega)$ given by equation (14). The parameters are $\epsilon_0 = 0, v_{L,R} = v, \beta_{L,R} = \beta = 1$. Left panel: E_p versus γ_0 for different couplings v to the leads. For weak coupling, the electron stays long enough in the molecule to obtain a full polaron shift $E_p^0 = -\gamma_0^2/\omega_0$. For increasing v, the residence time decreases and one gets an intermediate polaron shift $|E_p| < |E_p^0|$. For strong e–ph and v couplings, a deviation from $E_p \propto E_p^0$ is obtained. *Right panel*: E_p/E_p^0 versus the coupling v for different values of γ_0 and ω_0. For weak coupling ($v^2 < \omega_0/4$), the full polaron shift is obtained ($E_p/E_p^0 \sim 1$). When v increases, the electron residence time decreases as well as the polaron shift. The polaron shift has almost vanished for $v^2 > 3\beta\omega_0$. A scaling law $E_p/E_p^0 \sim f(v/\sqrt{\beta\omega_0})$ is obtained.

5. Temperature effects on the conductance peaks

In our previous studies on long conjugated molecular wires [42, 41], we have shown that the vibration modes that are the most strongly coupled to an injected charge carrier are the longitudinal optic phonon modes. We have also identified the mechanisms of charge injection and transport in such molecular wires. The transport is associated with the formation and propagation of polarons in semiconducting molecular wires [41]. More complex mechanisms arise in the presence of mid-gap states associated with a soliton defect [42]. All these studies were performed in the low-temperature limit. We now present new results for the temperature dependence of the conductance through short molecular wires in relation to recent experiments [5].

In these experiments, performed on polyphenylene-based molecular wires, the transport properties were measured at room temperature and at very low temperature ($T \sim 30$ K) with a mechanically controlled breakjunction [5]. The conductance curves show a peak just above the region of very low conductance at small bias. At low temperature, the peak is asymmetric towards higher energies with a maximum width of ∼125 meV. At room temperature, this peak has a reduced amplitude and is more symmetric, with a bell-like shape of maximum width of ∼300 meV.

It is clear that such a temperature dependence cannot be explained solely by the broadening of the Fermi distributions of the electrodes. Such a broadening over kT is not sufficient to

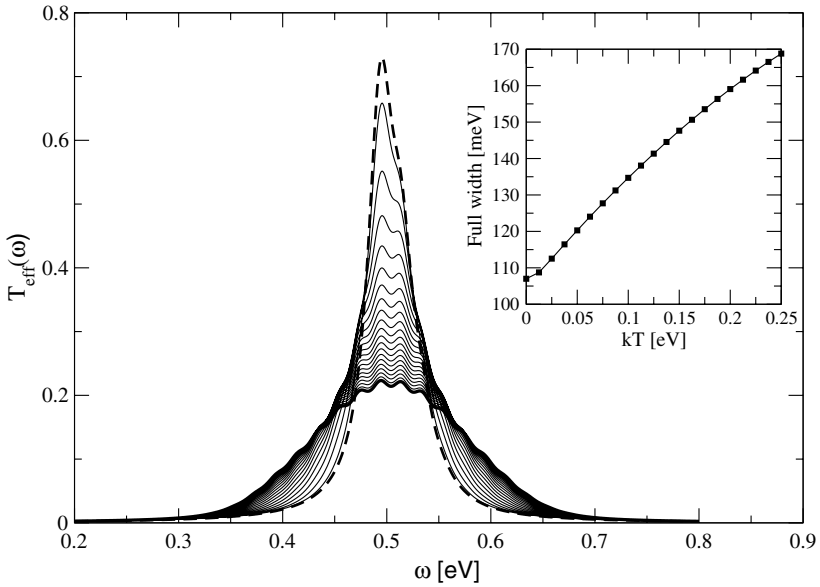

Figure 3. Total effective transmission $T_{\rm eff}(\omega)$ for different temperatures from $kT = 0$ (*dashed line*) to $kT = 12.5\omega_0$ (*solid line*) in steps of $\Delta kT/\omega_0 = 0.625$ (*thin solid lines*). The amplitude of the spectra decreases with increasing temperature. For very low temperatures, the transmission peak is asymmetric towards high energy because of the presence of phonon side-bands corresponding to phonon emission. As the temperature increases (room temperature $kT/\omega_0 \sim 1.25$ and above), both phonon emission and adsorption processes are available. The transmission peak becomes more symmetric around ϵ_0 and its amplitude decreases. The parameters for the SSSM model are $\epsilon_0/\beta = 0.5$, $\omega_0/\beta = 0.020$, $\gamma_0/\beta = 0.014$, $\upsilon/\beta = 0.087$ with $\upsilon_{\rm L,R} = \upsilon$ and $\beta_{\rm L,R} = \beta$. Calculations performed with a maximum vibration occupancy of $n_{\rm ph}^{\rm max} = 61$. *Inset:* temperature dependence of the width of the transmission peak.

explain the increase of the width of the conductance peak and is certainly not responsible for the modifications of the shape of the conductance peak. It is therefore reasonable to assume that there are some fluctuations inside the junction or at the molecule–lead contacts [65]. Considering the energy scale involved, such fluctuations can be related to low-frequency vibration modes, which may correspond to the centre of mass or libration vibration modes [65]. It is not straightforward to identify the exact nature of such modes; therefore, we consider a model system: the SSSM model.

We have performed calculations of the transmission according to the prescriptions given in section 3 for a broad range of values for the parameters and for the temperature. In the following, we present the results obtained for a single set of parameters which best fits the experiments.

Within the SSSM model, the single molecular level is taken to be $\epsilon_0 = 0.5$ eV, which corresponds to the position of the conductance peak observed in the experiments [5]. This molecular level is coupled to a low-frequency vibration mode ($\omega_0 \sim 20$ meV in agreement with recent numerical calculations [65]) via an e–ph coupling constant ($\gamma_0 \sim \omega_0/2$). The total effective transmission $T_{\rm eff}(\omega)$ is calculated as the sum of all the elastic and inelastic contributions for the different temperatures as described in section 3.1.

Figure 3 shows the transmission $T_{\rm eff}$ calculated for different temperatures ranging from the low-temperature limit ($kT = 0$) to the high-temperature limit ($kT/\omega_0 = 12.5$). In the

absence of e–ph coupling, the transmission is simply given by a single Breit–Wigner symmetric resonance located around ϵ_0 as expected. In the presence of e–ph coupling, the shape of the resonance is modified by the phonon side-band peaks. For very low temperatures, the transmission peak is asymmetric towards higher energy. The phonon side-band peaks are located at energies above ϵ_0 because only phonon emission processes are allowed at low temperatures. At room temperature and above, both phonon emission and adsorption processes become possible and the phonon side-band peaks appear for energies above and below the molecular level ϵ_0. The transmission peak is then broadened and more symmetric around ϵ_0.[3] Furthermore, the amplitude of the transmission peak is also reduced in comparison to the transmission obtained at $T = 0$ as observed experimentally.

It is interesting to note that similar lineshapes can be obtained for very low temperature and very strong e–ph coupling [79]. Such similarities between the lineshape functions for strong coupling at low temperature (where only phonon emission is possible) and the lineshape functions for medium to weak coupling at higher temperatures (where both phonon emission and adsorption are available) is only superficial as pointed out in [52], the physics in the two different regimes being quite different.

Now, by defining a probability distribution $p(\omega)$ from the transmission as $p(\omega) = T_{\mathrm{eff}}(\omega)/\int T_{\mathrm{eff}}(\omega)\,\mathrm{d}\omega$, one can calculate the corresponding different moments. The inset in figure 3 shows the effective full width of the conductance peak obtained from the second moment of $p(\omega)$. The width of the resonance increases with the temperature, almost linearly for large temperatures. Such a behaviour can be related to the temperature dependence of the mean square displacement of a harmonic oscillator.

Furthermore, such numerical results are in qualitative agreement with the temperature dependence of the width of the conductance peak measured from IETS spectra [21]. Therefore, one could in principle be able to extract the values of the intrinsic width or of the local effective temperature from the measurements.

However, it should be noticed that for all the calculations we have performed to obtain transmission shapes similar to the experiments[4] the temperatures used in the calculations are always larger than the room temperature. This behaviour may be related to a local heating effect in the molecular junction. Indeed, it is known that the effective temperature of molecular junctions could be substantially higher than the temperature of the surrounding system [80]. Furthermore, the local environment of the conducting molecule (neglected in the SSSM model) may also play an important role. Single-molecule junctions, where thermal conduction and other relaxation processes are limited, will generally exhibit a higher local temperature than a molecule embedded in a dense monolayer [23].

To conclude this section, it is interesting to note that a few-parameter model such as the SSSM model provides results that are in qualitative agreement with the conductance measurements performed in [5]. Therefore, the mechanism described by such a model provides a plausible explanation of the temperature dependence of the conductance peaks in molecular junctions. However, further investigations are needed to check the relevance/importance of other mechanisms such as hot-phonon effects or non-equilibrium fluctuation of the molecular level population [54, 56, 57].

[3] A similar increase of the level broadening has also been obtained in the limit of weak coupling to low-energy acoustic phonons in the somewhat different context of transport through quantum well [54].

[4] Such transmission lineshapes are obtained for a broad range of values for γ_0, ω_0 and $v_{\mathrm{L,R}}$ for which the broadening of the phonon side-band peaks due to the coupling to the leads is rather large. Each phonon side-band peak m overlaps with the adjacent broadened phonon side-band peaks $m \pm 1$. Figure 3 shows the results obtained for only one set of all the calculations.

6. Conclusion

In this paper, we have described an efficient method based on inelastic scattering to study the effects of electron–vibration coupling on the transport properties of molecular nanojunctions. We have briefly recalled the principal ingredients of the multi-channel inelastic scattering technique. We have also shown how this technique is connected to other approaches based on the single-particle approximation or two-particle Green's functions for non-interacting electrons and on non-equilibrium Green's functions using lowest-order expansions for the electron–phonon coupling. Our results corroborate the important idea that the Landauer picture *conductance is transmission probability* is still valid in the presence of interaction, as also recently shown by Imry *et al* [67].

In this paper, we have also discussed in detail the validity of different approximations used in the different models. For example, we have shown the effects of the lead self-energy on the transmission and we have studied another important physical effect, namely the dynamical polaron shift. We have shown the different regions of parameter space where the polaron shift effect can be neglected and where it should be retained.

As a practical application of the technique, we have provided a plausible explanation for the temperature dependence of the width and the shape of conductance peaks in molecular nanojunctions. The explanation relies on the inelastic and thermal excitation of low-frequency vibration modes in the junction. The results of the calculations for a model system are in good agreement with the measurements performed recently on single-molecule nanojunctions [5].

Extensions of the present technique to more realistic systems are under study. Preliminary calculations have shown the necessity of understanding the features in inelastic electron tunnelling spectroscopy by going beyond the single-vibration mode analysis [46]. Finally, the effects of multi-phonon excitations, the validity of perturbative treatments of the e–ph coupling in molecular wires, and a comparative study of lowest order expansions for the e–ph coupling in non-equilibrium Green's functions will be presented in forthcoming papers.

Appendix A. The current from the Green's functions

Let us consider a scattering region (a dot or a molecule which is described by a complete set of single-particle states and which can include interactions between particles) that is connected to two (left L and right R) leads described by non-interacting Fermi seas at their own equilibrium (characterized by the Fermi distributions f_{L} and f_{R}). The current J_{L} flowing from the left lead into the central region is expressed in terms of three Green's functions (the retarded G^{r}, advanced G^{a} and lesser $G^{<}$ Green's functions) of the interacting central region. In the stationary regime and for non-explicitly time-dependent problems, the current J_{L} is given by [81]

$$J_{\mathrm{L}} = \frac{\mathrm{i}e}{h} \int \mathrm{d}\omega \, \mathrm{Tr} \left\{ f_{\mathrm{L}}(\omega) \, \Gamma_{\mathrm{L}}(\omega) [G^{\mathrm{r}}(\omega) - G^{\mathrm{a}}(\omega)] + \Gamma_{\mathrm{L}}(\omega) \, G^{<}(\omega) \right\}, \tag{A.1}$$

where the trace runs on the single-particle states of the central region and Γ_{L} is related to the imaginary part of the retarded (advanced) self-energy $\Sigma_{\mathrm{L}}^{\mathrm{r(a)}}$ arising from the coupling of the central region to the left lead. These self-energies are included in the calculation of Green's functions $G^{\mathrm{r(a)}}$ via usual Dyson-like equations. Other self-energies arising from other kinds of interaction should also be included in $G^{\mathrm{r,a,<}}$.

An expression similar to equation (A.1) is obtained for the current J_{R} flowing from the right lead into the central region by interchanging the subscript L $\leftrightarrow$ R in equation (A.1). For

a current conserving system $J_L = -J_R$ and one can derive a symmetrized expression for the current by calculating $J = \frac{1}{2}(J_L - J_R)$ [81].

For identical L and R leads, the local density of states $\rho_{L,R}(\omega)$ at the sites connected to the central region (via the hopping integrals $V_{L,R}$) are identical. For a single-site connection and for energy-independent hopping integrals, the lead spectral functions $\Gamma_{L,R} \propto V^{\dagger}_{L,R}\rho_{L,R}(\omega)V_{L,R}$ are simply proportional to each other. In general when the coupling of the central region to the leads is given by a set of energy-independent hopping integrals, there always exists a transformation that links Γ_L to Γ_R [78]. In the following, we simply assume that $\Gamma_L(\omega) = \alpha\Gamma_R(\omega)$.

The current J can be evaluated from any linear combinations of J_L and J_R [54, 81] such as $J = \frac{a}{a+b}J_L - \frac{b}{a+b}J_R$ where $a, b \in \Re$ and $a + b \neq 0$. By taking $a = 1, b = \alpha$ one finds

$$J = \frac{ie}{h}\int d\omega\ \mathrm{Tr}\left\{\Gamma_L(\omega)\,[G^r(\omega) - G^a(\omega)](f_L(\omega) - f_R(\omega))\,\frac{1}{1+\alpha}\right\}$$
$$= \frac{ie}{h}\int d\omega\ \mathrm{Tr}\left\{\Gamma_R(\omega)\,[G^r(\omega) - G^a(\omega)](f_L(\omega) - f_R(\omega))\,\frac{\alpha}{1+\alpha}\right\}. \tag{A.2}$$

Therefore, the current through the junction is

$$J = -\frac{2e}{h}\int d\omega\,(f_L(\omega) - f_R(\omega))\,\mathrm{Im}\,\mathrm{Tr}\{\Gamma(\omega)\,G^r(\omega)\}, \tag{A.3}$$

where we used $G^r - G^a = 2i\,\mathrm{Im}\,G^r$ and

$$\Gamma(\omega) = \Gamma_L(\omega)\frac{1}{1+\alpha} = \Gamma_R(\omega)\frac{1}{1+1/\alpha} = \frac{\Gamma_L(\omega)\Gamma_R(\omega')}{\Gamma_L(\omega') + \Gamma_R(\omega')}. \tag{A.4}$$

It is important to note that the energies ω and ω' in the above expression for $\Gamma(\omega)$ are not necessarily equal to each other. This is an important result which is used to link the series expansion of the Green's function G^r to the transmission probabilities $T_{ab}(\omega', \omega)$ in section 3.1. Indeed, for the SSSM model at low temperature, one has

$$\mathrm{Im}\,\mathrm{Tr}\{\Gamma(\omega)\,G^r(\omega)\} = \Gamma(\omega)\ \mathrm{Im}\langle\chi_0|G^r|\chi_0\rangle = \Gamma(\omega)\ \sum_n \mathrm{Im}\,\Sigma^r_{\{n\}}|\langle\chi_n|G^r|\chi_0\rangle|^2$$
$$= \Gamma_L(\omega)\ \sum_n \Gamma_R(\omega - n\omega_0)|\langle\chi_n|G^r|\chi_0\rangle|^2, \tag{A.5}$$

where we used the properties of the lead self-energies $\mathrm{Im}\,\Sigma^r_{\{n\}}(\omega) = (\Gamma_R + \Gamma_L)(\omega - n\omega_0)$. The last line in equation (A.5) is simply the sum of the transmission probabilities $T_{ab}(\omega', \omega) = \Gamma_L(\omega)\Gamma_R(\omega')|\langle G^r_{ab}\rangle|^2$ given by equation (8) with $a \equiv |\chi_n\rangle$, $b \equiv |\chi_0\rangle$ and $\omega' = \omega - n\omega_0$.

Appendix B. The wide-band approximation and derivation of equation (18)

Let us start with equation (17)

$$\mathrm{Im}\,G^r_{00}(\omega) = -\Gamma\sum_n\left|\sum_{l=0}^{\infty}\langle\chi_n|\tilde{\chi}_l\rangle\frac{1}{\omega - \tilde{\epsilon}_0 - l\omega_0 + i\Gamma}\langle\tilde{\chi}_l|\chi_0\rangle\right|^2, \tag{B.1}$$

where $|\tilde{\chi}_n\rangle = U|\chi_n\rangle$ are the states of the displaced harmonic oscillator and $U = \exp g(a_0 - a_0^{\dagger})$ with $g = \gamma_0/\omega_0$. $\tilde{\epsilon}_0 = \epsilon_0 - g^2\omega_0$ is the electronic level displaced by the full polaron shift $-g^2\omega_0$.

It should be noted that the transformation U diagonalizes only the isolated molecule SSSM Hamiltonian. In the derivation of the full Green's functions, one should take into

account the effects of U on the lead self-energies. In the wide-band approximation, such renormalization effects are neglected. The lead self-energies entering the Green's functions are complex numbers $-\mathrm{i}\Gamma$ corresponding to a homogeneous broadening of the Green's functions' poles.

One can calculate the overlap between the harmonic states $|\chi_n\rangle$ and the displaced harmonic states $|\tilde{\chi}_l\rangle$. The lowest n terms are

$$\langle\chi_0|\tilde{\chi}_l\rangle = \frac{g^l}{\sqrt{l!}}\mathrm{e}^{-g^2/2},$$
$$\langle\chi_1|\tilde{\chi}_l\rangle = -g\langle\chi_0|\tilde{\chi}_l\rangle + \sqrt{l}\langle\chi_0|\tilde{\chi}_{l-1}\rangle = \langle\chi_0|\tilde{\chi}_l\rangle\ g\ (-1+l/g^2),$$
$$\langle\chi_2|\tilde{\chi}_l\rangle = \frac{1}{\sqrt{2}}\left(g^2\langle\chi_0|\tilde{\chi}_l\rangle - 2g\sqrt{l}\ \langle\chi_0|\tilde{\chi}_{l-1}\rangle - \sqrt{l(l-1)}\ \langle\chi_0|\tilde{\chi}_{l-2}\rangle\right)$$
$$= \langle\chi_0|\tilde{\chi}_l\rangle\ \frac{g^2}{\sqrt{2}}(1-2l/g^2+l(l-1)/g^4),$$

and

$$\langle\chi_n|\tilde{\chi}_l\rangle = \langle\chi_0|\tilde{\chi}_l\rangle\ \frac{g^n}{\sqrt{n!}}\sum_{k=0}^{n}(-1)^{k+l}\frac{1}{k!}\frac{n!}{(n-k)!}\frac{l!}{(l-k)!}g^{-2k} \qquad \text{for } n < l. \tag{B.2}$$

More generally, the overlaps $\langle\chi_m|\tilde{\chi}_n\rangle$ for any n, m are given by [82]

$$\langle\chi_m|\tilde{\chi}_n\rangle = \sqrt{n!\,m!}\,\mathrm{e}^{-g^2/2}\ g^{n+m}(-1)^n\sum_{k=0}^{\min(n,m)}\frac{(-1)^k\ (g^2)^{-k}}{k!(n-k)!(m-k)!}. \tag{B.3}$$

Using the definition of the associated Laguerre polynomials $L_n^{m-n}(x)$ [83], the expression for the overlap $\langle\chi_m|\tilde{\chi}_n\rangle$ can be rewritten as follows [84]:

$$\langle\chi_m|\tilde{\chi}_n\rangle = \sqrt{\frac{q_<!}{q_>!}}\mathrm{e}^{-g^2/2}g^{q_>-q_<}L_{q_<}^{q_>-q_<}(g^2)\ (\mathrm{sgn}(m-n))^{q_>-q_<}, \tag{B.4}$$

where $q_< = \min(n,m)$ and $q_> = \max(n,m)$.

Equation (B.4) can also be obtained by working with the real space representation of the harmonic states $\langle x|\chi_n\rangle$ given in terms of Hermite polynomials $H_n(u)$. For the bare harmonic states, one has

$$\langle x|\chi_n\rangle = \chi_n(x) = \left(\frac{\beta^2}{\pi}\right)^{1/4}\frac{1}{\sqrt{n!2^n}}\ \mathrm{e}^{-\beta^2x^2/2}\ H_n(\beta x), \tag{B.5}$$

and for the displaced oscillator states $\langle x|\tilde{\chi}_n\rangle = \tilde{\chi}_n(x) = \chi_n(x-x_\mathrm{g})$ with $\frac{1}{2}\beta^2x_\mathrm{g}^2 = g^2$. One recovers equation (B.4) by using the integral for Gaussian-weighted overlaps between Hermite polynomials [83]:

$$\int \mathrm{d}x\,\mathrm{e}^{-x^2}H_m(x+y)H_n(x+z) = 2^n\pi^{1/2}m!z^{n-m}L_m^{n-m}(-2yz) \qquad \text{for } m \leqslant n. \tag{B.6}$$

From equation (B.3) or equation (B.4), the different terms n in the square modulus of equation (B.1) are (for $n > 0$)

$$n=1:\ \sum_{l=0}^{\infty}\langle\chi_1|\tilde{\chi}_l\rangle\frac{1}{\omega-\tilde{\epsilon}_0-l\omega_0+\mathrm{i}\Gamma}\langle\tilde{\chi}_l|\chi_0\rangle$$
$$= g\mathrm{e}^{-g^2}\sum_{l=0}^{\infty}\frac{g^{2l}}{l!}\left(\frac{1}{\omega-\tilde{\epsilon}_0-l\omega_0+\mathrm{i}\Gamma}-\frac{1}{\omega-\tilde{\epsilon}_0-(l+1)\omega_0+\mathrm{i}\Gamma}\right); \tag{B.7}$$

$$
\begin{aligned}
n=2:\ & \sum_{l=0}^{\infty}\langle\chi_2|\tilde{\chi}_l\rangle\frac{1}{\omega-\tilde{\epsilon}_0-l\omega_0+\mathrm{i}\Gamma}\langle\tilde{\chi}_l|\chi_0\rangle \\
&= \frac{1}{\sqrt{2}}\sum_{l=0}^{\infty}g^2\frac{|\langle\chi_0|\tilde{\chi}_l\rangle|^2}{\omega-\tilde{\epsilon}_0-l\omega_0+\mathrm{i}\Gamma}-\frac{1}{\sqrt{2}}\sum_{l=1}^{\infty}2g\sqrt{l}\frac{\langle\chi_0|\tilde{\chi}_{l-1}\rangle\langle\tilde{\chi}_l|\chi_0\rangle}{\omega-\tilde{\epsilon}_0-l\omega_0+\mathrm{i}\Gamma} \\
&\quad+\frac{1}{\sqrt{2}}\sum_{l=2}^{\infty}\sqrt{l(l-1)}\frac{\langle\chi_0|\tilde{\chi}_{l-2}\rangle\langle\tilde{\chi}_l|\chi_0\rangle}{\omega-\tilde{\epsilon}_0-l\omega_0+\mathrm{i}\Gamma} \\
&= \frac{g^2}{\sqrt{2}}\mathrm{e}^{-g^2}\sum_{l=0}^{\infty}\frac{g^{2l}}{l!}\left(\frac{1}{\omega-\tilde{\epsilon}_0-l\omega_0+\mathrm{i}\Gamma}\right)-2\,\frac{g^{2l}}{l!}\left(\frac{1}{\omega-\tilde{\epsilon}_0-(l+1)\omega_0+\mathrm{i}\Gamma}\right) \\
&\quad+\frac{g^{2l}}{l!}\left(\frac{1}{\omega-\tilde{\epsilon}_0-(l+2)\omega_0+\mathrm{i}\Gamma}\right). \qquad \text{(B.8)}
\end{aligned}
$$

By summing up and reorganizing all the terms, one obtains the final result, equation (18):

$$
\mathrm{Im}\,G^{\mathrm{r}}_{00}(\omega)=-\Gamma\mathrm{e}^{-2g^2}\sum_{n=0}^{\infty}\frac{g^{2n}}{n!}\left|\sum_{j=0}^{n}(-1)^j\binom{n}{j}\sum_{l=0}^{\infty}\frac{g^{2l}}{l!}\frac{1}{\omega-\tilde{\epsilon}_0-(j+l)\omega_0+\mathrm{i}\Gamma}\right|^2. \qquad \text{(B.9)}
$$

To conclude this appendix, let us note that one could have worked in the subspace of the displaced harmonic oscillators to determine $\mathrm{Im}\,G^{\mathrm{r}}_{00}(\omega)$ as follows [85]:

$$
\begin{aligned}
\mathrm{Im}\,G^{\mathrm{r}}_{00}(\omega) &= \mathrm{Im}\langle\chi_0|\sum_n\frac{|\tilde{\chi}_n\rangle\langle\tilde{\chi}_n|}{\omega-\tilde{\epsilon}_0-n\omega_0+\mathrm{i}\Gamma}|\chi_0\rangle \\
&= \sum_n|\langle\tilde{\chi}_n|\chi_0\rangle|^2\frac{-\Gamma}{(\omega-\tilde{\epsilon}_0-n\omega_0)^2+\Gamma^2}=-\Gamma\,\mathrm{e}^{-g^2}\sum_n\frac{g^{2n}/n!}{(\omega-\tilde{\epsilon}_0-n\omega_0)^2+\Gamma^2}. \qquad \text{(B.10)}
\end{aligned}
$$

Equation (B.10) is simpler but strictly equivalent to equation (B.9) as shown in figure 1.

One should note that the equivalence between the different methods (the multi-channel scattering technique, the model derived by Wingreen *et al* [68] and equation (B.10)) is only valid in the wide-band approximation. Within this approximation, one can solve the transport problem by first applying the unitary transformation U to the isolated molecule and then by connecting the molecule to the leads; i.e., one considers that there is no effect of applying such a canonical transformation on the properties of the leads and of the matrix elements that couple the molecule to the leads. It is then easier to apply the techniques of Keldysh contour and non-equilibrium Green's functions to the SSSM model, as done for example in [75].

However in the most general cases, the wide-band limit is a quite poor approximation. As shown in figure 1, the energy dependence of the lead self-energies is very important, especially when the contacts between the molecule and the leads are made via some kind of clusters whose local density of states presents strong features on a small energy scale around the Fermi level. In such cases, one has to solve the problem by considering the correct energy dependence of the lead self-energies and the associated effects when one changes from one basis set to the other (i.e. swapping between the basis set $|\chi_n\rangle$ and $|\tilde{\chi}_n\rangle$ in the SSSM model).

Furthermore, by working within the wide-band approximation, one works in a limited region of the parameter space where the interesting physics of the dynamical polaron shift is omitted as described in section 3.1. Indeed, within the wide-band approximation, the electronic level is shifted by the full polaron shift $\tilde{\epsilon}_0=\epsilon_0-g^2\omega_0$ for all energies considered.

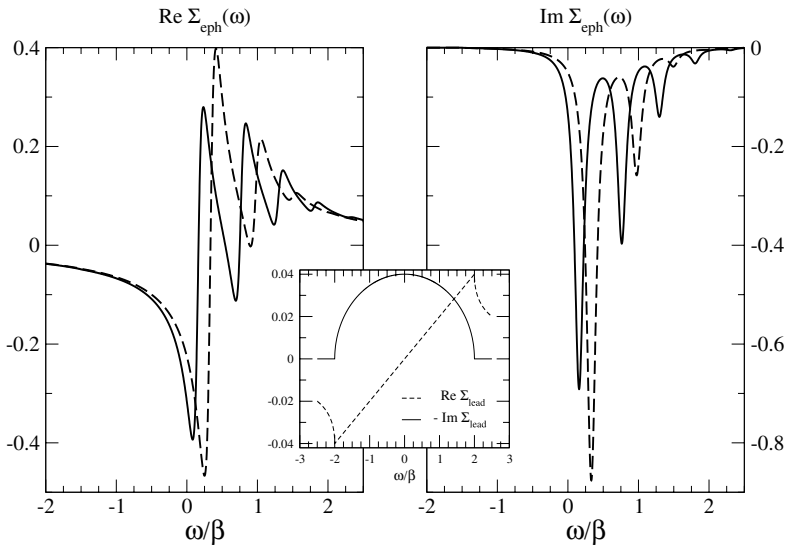

Figure C.1. Real (*left panel*) and imaginary (*right panel*) parts of the self-energy $\Sigma^{\rm r}_{\rm eph}(\omega)$ calculated from equation (C.8) (*dashed lines*) and from the exact expression equation (C.2) (*solid lines*). The real and imaginary parts of the lead self-energy $\Sigma^{\rm r}_{\{0\}}(\omega)$ are given in the inset. The parameters for the SSSM model are $\epsilon_0/\beta = 0$, $\omega_0/\beta = 0.5$, $\gamma_0/\beta = 0.3$, $v/\beta = 0.2$ with $v_{\rm L,R} = v$ and $\beta_{\rm L,R} = \beta = 1$. Calculations are performed with a maximum vibration occupancy of $n^{\rm max}_{\rm ph} = 17$.

Appendix C. Derivation of the self-energy $\Sigma_{\rm eph}(\omega)$

The retarded electronic Green's function in equation (14) can be rewritten in a more compact form as follows:

$$G^{\rm r}(\omega) = [\,\omega - \epsilon_0 - \Sigma^{\rm r}_{\{0\}}(\omega) - \Sigma^{\rm r}_{\rm eph}(\omega)]^{-1}, \tag{C.1}$$

where we have introduced the self-energy $\Sigma^{\rm r}_{\rm eph}(\omega)$ due to the e–ph interaction. From equation (14), this self-energy is expressed as the following continued fraction:

$$\Sigma^{\rm r}_{\rm eph}(\omega) = \cfrac{\gamma_0^2}{G^{\rm r}_0(\omega-\omega_0)^{-1} - \cfrac{2\,\gamma_0^2}{G^{\rm r}_0(\omega-2\omega_0)^{-1} - \cfrac{3\,\gamma_0^2}{G^{\rm r}_0(\omega-3\omega_0)^{-1} - \cdots}}} \tag{C.2}$$

where $G^{\rm r}_0(\omega)$ is the retarded Green's function of the molecule connected to the leads in the absence of e–ph interaction $G^{\rm r}_0(\omega) = [\omega - \epsilon_0 - \Sigma^{\rm r}_{\{0\}}(\omega)]^{-1}$.

Note that by using the properties of the lead self-energies, $\Sigma^{\rm r}_{\{n\}}(\omega) = \Sigma^{\rm r}_{\{0\}}(\omega - n\omega_0)$, one has $G^{\rm r}_0(\omega - n\omega_0)^{-1} = \omega - \epsilon_0 - n\omega_0 - \Sigma^{\rm r}_{\{0\}}(\omega - n\omega_0) = \omega - \epsilon_0 - n\omega_0 - \Sigma^{\rm r}_{\{n\}}(\omega)$.

It can be shown [78] that the continued-fraction expansion of $\Sigma^{\rm r}_{\rm eph}$ can be reformulated as a series expansion in terms of the powers of the e–ph coupling γ_0:

$$\Sigma^{\rm r}_{\rm eph}(\omega) = \sum_n \Sigma^{{\rm r},(n)}_{\rm eph}(\omega, \mathcal{O}[\gamma_0^{2n}]). \tag{C.3}$$

In such a series expansion, the lowest order term is

$$\Sigma^{{\rm r},(1)}_{\rm eph}(\omega) = \gamma_0^2\, G^{\rm r}(\omega - \omega_0). \tag{C.4}$$

The self-energy $\Sigma^{r,(1)}_{eph}$ is related to the e–ph self-energy obtained at low temperature for the self-consistent Born approximation [57–59, 61, 62].

The higher order terms correspond to multiple phonon excitations [78]. For example, the term in $\mathcal{O}[\gamma_0^4]$ is

$$\Sigma^{r,(2)}_{eph}(\omega) = \gamma_0^4\, G^r(\omega-\omega_0)G^r(\omega-2\omega_0)G^r(\omega-\omega_0), \tag{C.5}$$

higher order terms in $\mathcal{O}[\gamma_0^6]$ are

$$\Sigma^{r,(3a)}_{eph}(\omega) = \gamma_0^6 G^r(\omega-\omega_0)G^r(\omega-2\omega_0)G^r(\omega-3\omega_0)G^r(\omega-2\omega_0)G^r(\omega-\omega_0), \tag{C.6}$$

and

$$\Sigma^{r,(3b)}_{eph}(\omega) = \gamma_0^6 G^r(\omega-\omega_0)G^r(\omega-2\omega_0)G^r(\omega-\omega_0)G^r(\omega-2\omega_0)G^r(\omega-\omega_0). \tag{C.7}$$

A similar series expansion of the e–ph self-energy can also be obtained by using a linked cluster expansion approach [86].

In the limit of weak e–ph interaction ($\gamma_0 \ll 1$), the leading term of the series is obviously the lowest-order term $\Sigma^{r,(1)}_{eph}$ related to the self-consistent Born approximation [57–59, 61, 62]. In the other cases (medium to strong e–ph coupling), the higher-order terms are important and need to be included in the calculations in order to correctly reproduce the multi-phonon excitations.

Finally, one should note that by inserting the expression equation (C.4) into the definition of G^r in equation (C.1) one can expand the e–ph self-energy as

$$\Sigma^r_{eph}(\omega) = \cfrac{\gamma_0^2}{G^r_0(\omega-\omega_0)^{-1} - \cfrac{\gamma_0^2}{G^r_0(\omega-2\omega_0)^{-1} - \cfrac{\gamma_0^2}{G^r_0(\omega-3\omega_0)^{-1} - \cdots}}} \tag{C.8}$$

However, equation (C.8) is not the correct expansion for the e–ph self-energy. The exact continued-fraction expansion of Σ^r_{eph} includes a factor n at each level of the expansion as can be seen in equation (C.2). Such factors arise when applying the creation (annihilation) phonon operator on the corresponding vibration state $|\chi_{n-1(n)}\rangle$ in a multi-excitation process. The absence of the factors n generates a wrong self-energy as can be seen in figure C.1. The positions of the peaks in the real and imaginary parts of the self-energy as well as their amplitudes are incorrect when one calculates Σ^r_{eph} with equation (C.8) instead of using the exact expression equation (C.2).

Such an incorrect energy dependence of the self-energy also generates wrong features in the corresponding effective transmission. These effects will be analysed in detail in a forthcoming paper. However, one can already say that the polaron shift observed in the transmission is not correctly reproduced when one omits the n factors in the self-energy. Furthermore, the high energy peaks in the effective transmission appear at energies $\omega = m\omega_0$, which gives wrong energy differences between the first zero-phonon peak and the other phonon side-band peaks. Such an incorrect transmission lineshape is not obtained when the factors n are properly included in the continued-fraction expansion equation (C.2).

References

[1] Joachim C and Ratner M A 2005 *Proc. Natl Acad. Sci. USA* **102** 8801
[2] Joachim C and Ratner M A 2004 *Nanotechnology* **15** 1065
[3] Nitzan A and Ratner M A 2003 *Science* **300** 1384
[4] Reed M A and Lee T (ed) 2003 *Molecular Nanoelectronics* (Stevenson Ranch, California: American Scientific Publishers)

[5] Reichert J, Weber H B, Mayor M and Löhneysen H V 2003 *Appl. Phys. Lett.* **82** 4137
[6] Dulić D, van der Molen S J, Kudernac T, Jonkman H T, de Jong J J D, Bowden T N, van Esch J, Feringa B L and van Wees B J 2003 *Phys. Rev. Lett.* **91** 207402
[7] Piva P G, DiLabio G A, Pitters J L, Zikovsky J, Rezeq M, Dogel S, Hofer W A and Wolkow R A 2005 *Nature* **435** 658
[8] Elbing M, Ochs R, Koentopp M, Fischer M, von Hänisch C, Weigend F, Evers F, Weber H B and Mayor M 2005 *Proc. Natl Acad. Sci. USA* **102** 8815
[9] Gao B, Chen Y F, Fuhrer M S, Glattli D C and Bachtold A 2005 *Phys. Rev. Lett.* **95** 196802
[10] Dujardin E, Derycke V, Goffman M F, Lefèvre R and Bourgoin J P 2005 *Appl. Phys. Lett.* **87** 193107
[11] Park J, Pasupathy A N, Goldsmith J I, Chang C, Yaish Y, Petta J R, Rinkoski M, Sethna J P, Abruña H D, McEuen P L and Ralph D C 2002 *Nature* **417** 722
[12] Liang W, Shores M P, Bockrath M, Long J R and Park H 2002 *Nature* **417** 725
[13] Porath D, Bezryadin A, de Vries S and Decker C 2000 *Nature* **403** 635
[14] Endres R G, Cox D L and Singh R R P 2004 *Rev. Mod. Phys.* **76** 195
[15] Xu B, Zhang P, Li X and Tao N 2004 *Nano Lett.* **4** 1105
[16] Hu W, Jiang J, Nakashima H, Luo Y, Kashimura Y, Chen K Q, Shuai Z, Furukawa K, Lu W, Liu Y, Zhu D and Torimitsu K 2006 *Phys. Rev. Lett.* **96** 027801
[17] Ho W 2002 *J. Chem. Phys.* **117** 11033
[18] Liu N, Pradhan N A and Ho W 2004 *J. Chem. Phys.* **120** 11371
[19] Park H, Park J, Lim A K L, Anderson E H, Alivisatos A P and McEuen P L 2000 *Nature* **407** 57
[20] Kushmerick J G, Lazorcik J, Patterson C H and Shashidhar R 2004 *Nano Lett.* **4** 639
[21] Wang W, Lee T, Kretzschmar I and Reed M A 2004 *Nano Lett.* **4** 643
[22] Yu L H, Keane Z K, Ciszek J W, Cheng L, Stewart M P, Tour J M and Natelson D 2004 *Phys. Rev. Lett.* **93** 266802
[23] Selzer Y, Cai L, Cabassi M A, Yao Y, Tour J M, Mayer T S and Allara D L 2005 *Nano Lett.* **5** 61
[24] Heeger A J 2001 *Rev. Mod. Phys.* **73** 681
[25] Heeger A J, Kivelson S, Schrieffer J R and Su W P 1988 *Rev. Mod. Phys.* **60** 781
[26] Persson B N J and Baratoff A 1987 *Phys. Rev. Lett.* **59** 339
[27] Lorente N and Persson M 2000 *Phys. Rev. Lett.* **85** 2997
[28] Lorente N and Persson M 2000 *Faraday Discuss.* **117** 277
[29] Lorente N, Persson M, Lauhon L J and Ho W 2001 *Phys. Rev. Lett.* **86** 2593
[30] Montgomery M J and Todorov T N 2003 *J. Phys.: Condens. Matter* **15** 8781
[31] Montgomery M J, Hoekstra J, Sutton A P and Todorov T N 2003 *J. Phys.: Condens. Matter* **15** 731
[32] Montgomery M J, Todorov T N and Sutton A P 2002 *J. Phys.: Condens. Matter* **14** 5377
[33] Chen Y C, Zwolak M and di Ventra M 2005 *Nano Lett.* **5** 621
[34] Chen Y C, Zwolak M and di Ventra M 2005 *Nano Lett.* **4** 1709
[35] di Ventra M, Chen Y C and Zwolak M 2003 *Nano Lett.* **3** 1691
[36] Sols F 1992 *Ann. Phys.* **214** 386
[37] Bonča J and Trugman S A 1995 *Phys. Rev. Lett.* **75** 2566
[38] Ness H and Fisher A J 1999 *Phys. Rev. Lett.* **83** 452
[39] Haule K and Bonča J 1999 *Phys. Rev.* B **59** 13087
[40] Mingo N and Makoshi K 2000 *Phys. Rev. Lett.* **84** 3694
[41] Ness H, Shevlin S A and Fisher A J 2001 *Phys. Rev.* B **63** 125422
[42] Ness H and Fisher A J 2002 *Europhys. Lett.* **57** 885
[43] Troisi A, Ratner M A and Nitzan A 2003 *J. Chem. Phys.* **118** 6072
[44] Troisi A and Ratner M A 2005 *Phys. Rev.* B **72** 033408
[45] Jiang J, Kula M, Lu W and Luo Y 2005 *Nano Lett.* **5** 1551
[46] Ness H and Fisher A J 2005 *Proc. Natl Acad. Sci. USA* **102** 8826
[47] Petrov E G, May V and Hänggi P 2004 *Chem. Phys.* **296** 251
[48] Nitzan A 2001 *Annu. Rev. Phys. Chem.* **52** 681
[49] Horsfield A P, Bowler D R, Fisher A J, Todorov T N and Sánchez C G 2005 *J. Phys.: Condens. Matter* **17** 4793
[50] Hliwa M and Joachim C 2002 *Phys. Rev.* B **65** 085406
[51] Caroli C, Combescot R, Nozieres P and Saint-James D 1972 *J. Phys. C: Solid State Phys.* **5** 21
[52] Mahan G D 1990 *Many-Particle Physics* (New York: Plenum)
[53] Anda E V and Flores F 1991 *J. Phys.: Condens. Matter* **3** 9087
[54] Král P, Sheard F W and Ouali F F 1998 *Phys. Rev.* B **57** 15428
[55] Mii T, Tikhodeev S and Ueba H 2002 *Surf. Sci.* **502/503** 26
[56] Mii T, Tikhodeev S and Ueba H 2003 *Phys. Rev.* B **68** 205406

[57] Galperin M, Ratner M A and Nitzan A 2004 *Nano Lett.* **4** 1605
[58] Galperin M, Ratner M A and Nitzan A 2004 *J. Chem. Phys.* **121** 11965
[59] Pecchia A, di Carlo A, Gagliardi A, Sanna S, Frauenhein T and Gutierrez R 2004 *Nano Lett.* **4** 2109
[60] Pecchia A and di Carlo A 2004 *Rep. Prog. Phys.* **67** 1497
[61] Asai Y 2004 *Phys. Rev. Lett.* **93** 246102
Asai Y 2004 *Phys. Rev. Lett.* **94** 099901 (erratum)
[62] Frederiksen T, Brandbyge M, Lorente N and Jauho A P 2004 *Phys. Rev. Lett.* **93** 256601
[63] Viljas J K, Cuevas J C, Pauly F and Häfner M 2005 *Phys. Rev.* B **72** 245415
[64] Yamamoto T, Watanabe K and Watanabe S 2005 *Phys. Rev. Lett.* **95** 065501
[65] Sergueev N, Roubtsov D and Guo H 2005 *Phys. Rev. Lett.* **95** 146803
[66] de la Vega L, Martín-Rodero A, Agraït N and Levy-Yeyati A 2006 *Phys. Rev.* B **73** 075428
[67] Imry Y, Entin-Wohlman O and Aharony A 2005 *Europhys. Lett.* **72** 263
[68] Wingreen N S, Jacobsen K W and Wilkins J W 1989 *Phys. Rev.* B **40** 11834
[69] Ness H and Gautier F 1995 *J. Phys.: Condens. Matter* **7** 6625
[70] Ness H and Gautier F 1995 *Phys. Rev.* B **52** 7352
[71] Yaliraki S and Ratner M A 1998 *J. Chem. Phys.* **109** 5036
[72] Ke S H, Baranger H U and Yang W 2005 *J. Chem. Phys.* **122** 074704
[73] Cuniberti G, Fagas G and Richter K 2002 *Chem. Phys.* **281** 465
[74] Lundin U and McKenzie R H 2002 *Phys. Rev.* B **66** 075303
[75] Chen Z, Lü R and Zhu B 2005 *Phys. Rev.* B **71** 165324
[76] Ness H and Fisher A J 1998 *J. Phys.: Condens. Matter* **10** 3697
[77] Paulsson M, Frederiksen T and Brandbyge M 2005 *Phys. Rev.* B **72** 201101
[78] Ness H 2006 unpublished
[79] Flensberg K 2003 *Phys. Rev.* B **68** 205323
[80] Selzer Y, Cabassi M A, Mayer T S and Allara D L 2004 *Nanotechnology* **15** S483
[81] Meir Y and Wingreen N S 1992 *Phys. Rev. Lett.* **68** 2512
[82] Katriel J 1970 *J. Phys. B: At. Mol. Phys.* **3** 1315
[83] Gradshteyn I S and Ryzhik I M 1965 *Table of Integrals, Series and Products* (New York: Academic)
[84] Cahill K E and Glauber R J 1969 *Phys. Rev.* **177** 1857
[85] Hewson A C and Newns D M 1980 *J. Phys. C: Solid State Phys.* **13** 4477
[86] Král P 1997 *Phys. Rev.* B **56** 7293